Available online at www.sciencedirect.com

ScienceDirect

Energy Procedia 45 (2014) 385 – 394

Energy Procedia

68th Conference of the Italian Thermal Machines Engineering Association, ATI2013

Three-dimensional CFD evaluation of the characterizing parameters in the fire/structure interaction

Assunta Andreozzi, Nicola Bianco, Marilena Musto*, Vincenzo Naso, Giuseppe Rotondo

Dipartimento di Ingegneria Industriale - Università degli Studi di Napoli Federico II - P.le Tecchio, 80 – 80125 – Napoli - Italy

Abstract

With reference to a steel beam located at the ceiling of a small room irradiated by a burner located on the floor, that is the fire source, the Adiabatic Surface Temperature (AST) has been evaluated. Surface temperatures of the beam and the heat fluxes released to it (conjugate case) are then compared to those in a single beam with the AST as boundary condition (standalone case). Results show that, by assuming AST as the exchange parameter between fire and structural models, differences between conjugate and standalone case are strongly dependent on the convection coefficient assumed in the latter one.

Keywords: adiabatic surface temperature, CFD analysis, thermal/structural parameter, fire safety, fire structure interaction.

Nomenclature

c_p	specific heat, J kg^{-1} K^{-1}	n	normal to the surface
$e_{\dot{q}_{tot}}$	total heat flux relative error, eq.(18)	p	pressure, Pa
e_{T_b}	surface temperature relative error, eq.(19)	Pr	Prandtl number
F_{i-w}	configuration factor	$\dot{q}$	heat flux, W m^{-2}
g	acceleration due to the gravity, m s^{-2}	s	direction of the irradiation
h	coefficient of convection, W m^{-2} K^{-1}	T	temperature, K
I	irradiation, W m^{-2}	u, v, w	velocity components, m s^{-1}
k	thermal conductivity, W m^{-1} K^{-1}	x, y, z	Cartesian coordinates, m

* Corresponding author. Tel.: +39 081 7682290; fax:+39 081 2390364
E-mail address: marilena.musto@unina.it

doi:10.1016/j.egypro.2014.01.042

Greek symbols		*f*	fluid
β	volumetric expansion coefficient, K^{-1}	*in*	incident
ε	emissivity	*out*	outgoing
μ	viscosity, Pa s	*p*	plasterboard
ρ	density, kg m^{-3}	*rad*	radiative
σ	Stephan-Boltzmann constant, W m^{-2} K^4	*req*	refers to temperature in eq.(3)
Ω	solid angle, sr	*s*	solid (beam/plasterboard)
Subscripts		*stan*	standalone
AST	adiabatic surface temperature	*t*	turbulent
b	beam	*tot*	total (radiative + convective)
con	convective	*w*	wall
conj	conjugate	*0*	ambient

1. Introduction

Fire Safety Engineering (FSE) is widely developed in last decades due to the building of large and complex structures. Computational Fluid Dynamics (CFD) codes and structural ones, based on Finite Element Methods (FEM), are employed to foresee the fire evolution and its effects on structures. Following the World Trade Center disaster, a number of authoritative organizations, such as Federal Emergency Management Authority (FEMA) [1] and Institution of Structural Engineer (ISE) [2], have identified joint integrity as a key to maintain structural integrity in fire and have called for extensive research on joints under fire conditions [3 - 6].

Conjugate CFD and structural analyses would be the best way to analyze the thermo-structural problem, since the fire evolution and the structural response are interconnected. However, the large computational resources required because of the different time and space scales necessary for the discretization of thermofluid-dynamic and structural problems make, nowadays, this approach impracticable.

Alternatively to the conjugate approach, thermofluid-dynamic and structural problems could be solved separately, by using appropriate boundary conditions to couple the two models. We can distinguish two main methodologies: "one way" in which only the data collected by a CFD code are transferred to the structural code, and "two-way" where even the data produced by an FEM code are returned to the fire model. The latter method is more accurate but requires more computational time. Within this approach, Noordijk et al. [7] have developed a complete interface between the VESTA ™ CFD code and the Diana ™ FEM code, but this approach requires large computational time due to the double transfer of data.

The "one-way" approach, which allows to reduce the computational time, could be used preferably when the dimensions of the structural elements and their displacement due to structure deformations are negligible compared to the size of the compartment. In this case it is possible to assume that the deformations of the elements due to thermal loads do not affect appreciably the evolution of the hot gases.

The exchange of information between the CFD and FEM codes is one of the open problems in FSE. It greatly influences both the accuracy of the solutions and the computational time. The European Community has funded a study on the different methods of coupling the two codes and on the data exchange format, called FIRESTRUCT [8]. Within this project, four different pairs of software CFD-FEM coupling have been compared ((JASMINE/SAFIR, VESTA/DIANA, FDS/ANSYS and JASMINE/STELA) with six different types of data exchange, providing indications for their use.

Franssen [9] performed a study on the "one-way" methodology, that compared data obtained through CFD-FEM analysis by using two types of algorithms for exchange parameters: the former proposed by Watson and Philip [10], called "natural neighbors" and the second, proposed by themselves, based on trilinear interpolation of thermal parameters in the nodal points where the fluid dynamics and structural discretizations overlap. Prasad and Baum [3] simulated, in a "one-way" mode, the response of a complex structure subjected to a fire, using the heat flux as parameter exchange between the CFD (Fire Dynamic Simulator) and the FEM codes. Ren et al. [11] developed a dynamic transfer to share data between FDS and ANSYS codes. Wickström et al. [12] defined the Adiabatic Surface Temperature (AST) as the exchange parameter between the CFD and FEM codes, for a two-dimensional problem by

using a one way approach. AST takes into account both convective and radiative heat fluxes, thus reducing the number of parameters to be used in coupling thermofluid-dynamic and structural models. Wickström et al. [13] and Bystrom et al. [14] made use of AST in the design of structures for fire exposure and in experiments of fire in a full scale compartment. Andreozzi et al. [15] investigated the use of the Adiabatic Surface Temperature (AST) in a two-dimensional problem, by using a one way approach. A comparison between the one-way model and the conjugate one pointed out errors in structure temperatures less than 2%.

In the present paper, the analysis presented in [15] has been extended to a three-dimensional case. A steel beam is located in a confined room where a fire scenario is simulated by assuming the presence of a burner at an assigned temperature located on the room floor in front of the beam, placed at the room ceiling. Beam surface temperatures are evaluated both in the "conjugate" case, by modelling the convective-radiative heat transfer in the room and the conductive heat transfer in the beam and in a "standalone" case, by modeling only heat conduction in the beam, imposing a third type boundary condition at beam boundaries. The AST, evaluated in the conjugate analysis, is assumed as the external temperature. Different convection coefficients are assumed on the beam walls.

Results are presented in terms of convection coefficients and temperature profiles at the beam walls both for the "conjugate" and "standalone" analyses. Relative errors between predictions obtained by means of the conjugate case and the standalone beam case are provided. The comparison between results obtained by means of the two proposed analyses shows that using AST as the transfer thermal parameter between CFD and FEM models leads to errors of the order of 2 % when convection coefficients evaluated in the conjugate case were used, while errors up to 75% were found when different convection coefficients were assumed.

2. The adiabatic surface temperature

In fire scenarios the total heat flux to the wall, $\dot{q}_{tot}$, is

$$\dot{q}_{tot} = \dot{q}_{rad} + \dot{q}_{con} \tag{1}$$

where $\dot{q}_{rad}$ is the net radiative heat flux to the wall and $\dot{q}_{con}$ is the convective heat flux between the fluid and the wall.

The net radiative heat flux, $\dot{q}_{rad}$, can be expressed as

$$\dot{q}_{rad} = \varepsilon_w \sigma \left(T_{req}^4 - T_w^4 \right) \tag{2}$$

with ε_w the emissivity of the wall, which is assumed to be a gray body, T_w the temperature of the wall surface and

$$T_{req}^4 = \sum_i \varepsilon_i \, F_{i-w} \, T_i^4 \tag{3}$$

that is the temperature of a uniform temperature black body with a unitary configuration factor to the wall.

The convective heat flux, $\dot{q}_{con}$, can be expressed as

$$\dot{q}_{con} = h \left(T_f - T_w \right) \tag{4}$$

with h the coefficient of convection and T_f the temperature of the fluid.

Therefore, the total net heat flux to the exposed wall can be expressed as:

$$\dot{q}_{tot} = \varepsilon_w \, \sigma \left(T_{req}^4 - T_w^4 \right) + h \left(T_f - T_w \right) \tag{5}$$

The adiabatic surface temperature, $T_{AST,}$ was defined by Wickström et al. [12] as the temperature assumed by a perfect insulator exposed to the same heating conditions as the real wall. The total net heat flux to this ideal surface is by definition zero and equation (5) becomes

$$\varepsilon_w \, \sigma\left(T_{req}^4 - T_{AST}^4\right) + h\left(T_f - T_{AST}\right) = 0 \tag{6}$$

Equation (6) shows that the adiabatic surface temperature can assume values in the $T_{req} \div T_f$ range. Wickström et al. [12] proposed to use T_{AST} as the transfer parameter from fire models to structural models. Thus, the T_{AST} predicted by a fire model or measured by a thin plate thermometer can be introduced in a structural model to take into account both radiative and convective heat fluxes to the exposed wall in the prediction of the thermal field inside solids

$$\dot{q}_{tot} = \varepsilon_w \, \sigma\left(T_{AST}^4 - T_w^4\right) + h\left(T_{AST} - T_w\right) \tag{7}$$

3. Mathematical description and numerical models

Reference is made to the small parallelepipedic enclosure, 2.48 m × 1.00 m × 2.00 m high, sketched in figure 1. The walls are made up of plasterboard, 0.020 m thick. Two couples of vents, 2.48 m long and 0.60 m high, are located at the top and the bottom of the 2.48 m long and 2.50 m high vertical walls. A steel IPE beam, equidistant from the above said lateral walls, is attached to the ceiling. Its dimensions are reported in figure 2 and table 1. Upon the floor, directly in front of the beam, the fire source is located, a burner 0.80 m × 0.80 m × 0.080 m high. The thermophysical properties of plasterboard, steel and air are reported in table 2.

3.1. Conjugate case

The three-dimensional computational domain is sketched in figure 3.

The following assumptions have been made:

- surfaces are gray;
- thermo-physical properties of the solids are constant with respect to the temperature;

Table 1. Dimensions of the IPE beam.

h (mm)	b (mm)	a (mm)	e (mm)	r (mm)	d (mm)
500	360	20	50	1	2,480

Table 2. Thermophysical properties of materials.

Material	ρ (kg m^{-3})	c_p (J kg^{-1} K^{-1})	k (W m^{-1} K^{-1})	μ (Pa s)	β (K^{-1})
Air	1.225	1,006	2.42×10^{-2}	1.789×10^{-5}	3.33×10^{-3}
Steel	8,030	502.5	16.3	-	-
Plasterboard	737	1,423	0.12	-	-

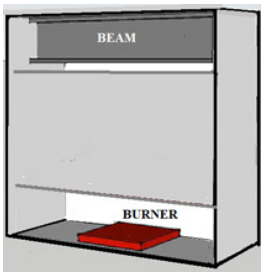

Fig.1. Sketch of the enclosure.

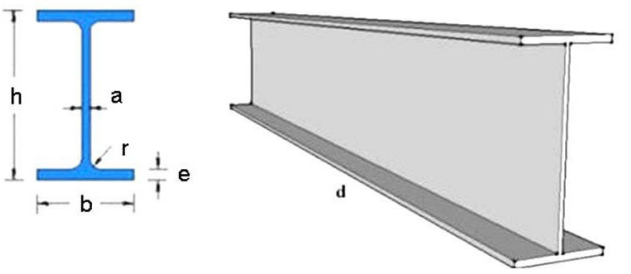

Fig.2. Sketch of the IPE beam.

- except for the air density, for which the ideal gas model is assumed, thermo-physical properties of the fluid are assumed to be independent of the temperature since radiation heat transfer between the burner and the beam is predominant and, then, no large fluid temperature increase is expected;
- properties, except the density, are evaluated at a 300 K temperature.

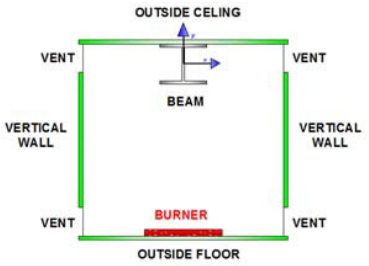

Fig.3. The computational domain for the conjugate case.

3.1.1. Equations governing the fluid domain

The governing equations, for the fluid region in steady state regime, are time-averaged mass, Navier-Stokes and energy equations combined with k-ε realizable turbulence model [16]. For the sake of simplicity, notations used in this study neglect the superscript bar usually employed to denote time-averaged dependent variables.

The modeled transport equations are:

$$\frac{\partial(\rho u)}{\partial x}+\frac{\partial(\rho v)}{\partial y}+\frac{\partial(\rho w)}{\partial z}=0 \tag{8}$$

$$\frac{\partial(\rho uu)}{\partial x}+\frac{\partial(\rho uv)}{\partial y}+\frac{\partial(\rho uw)}{\partial z}=-\frac{\partial p}{\partial x}+\frac{\partial}{\partial x}\left[(\mu+\mu_t)\frac{\partial u}{\partial x}\right]+\frac{\partial}{\partial y}\left[(\mu+\mu_t)\frac{\partial u}{\partial y}\right]+\frac{\partial}{\partial z}\left[(\mu+\mu_t)\frac{\partial u}{\partial z}\right] \tag{9}$$

$$\frac{\partial(\rho uv)}{\partial x}+\frac{\partial(\rho vv)}{\partial y}+\frac{\partial(\rho vw)}{\partial z}=-\frac{\partial p}{\partial y}+\frac{\partial}{\partial x}\left[(\mu+\mu_t)\frac{\partial v}{\partial x}\right]+\frac{\partial}{\partial y}\left[(\mu+\mu_t)\frac{\partial v}{\partial y}\right]+\frac{\partial}{\partial z}\left[(\mu+\mu_t)\frac{\partial v}{\partial z}\right]+ \tag{10}$$
$$+g\rho\beta(T_f-T_0)$$

$$\frac{\partial(\rho uw)}{\partial x}+\frac{\partial(\rho vw)}{\partial y}+\frac{\partial(\rho ww)}{\partial z}=-\frac{\partial p}{\partial z}+\frac{\partial}{\partial x}\left[(\mu+\mu_t)\frac{\partial w}{\partial x}\right]+\frac{\partial}{\partial y}\left[(\mu+\mu_t)\frac{\partial w}{\partial y}\right]+\frac{\partial}{\partial z}\left[(\mu+\mu_t)\frac{\partial w}{\partial z}\right] \tag{11}$$

$$\frac{\partial(\rho uT_f)}{\partial x}+\frac{\partial(\rho vT_f)}{\partial y}+\frac{\partial(\rho wT_f)}{\partial z}=\frac{\partial}{\partial x}\left[\left(\frac{k_f}{c_p}+\frac{\mu_t}{Pr_t}\right)\frac{\partial T_f}{\partial x}\right]+\frac{\partial}{\partial y}\left[\left(\frac{k_f}{c_p}+\frac{\mu_t}{Pr_t}\right)\frac{\partial T_f}{\partial y}\right]+\frac{\partial}{\partial z}\left[\left(\frac{k_f}{c_p}+\frac{\mu_t}{Pr_t}\right)\frac{\partial T_f}{\partial z}\right] \tag{12}$$

$$\frac{\partial(\rho\varepsilon u)}{\partial x}+\frac{\partial(\rho\varepsilon v)}{\partial y}+\frac{\partial(\rho\varepsilon w)}{\partial z}=\frac{\partial}{\partial x}\left[\left(\mu+\frac{\mu_t}{\sigma_\varepsilon}\right)\frac{\partial\varepsilon}{\partial x}\right]+\frac{\partial}{\partial y}\left[\left(\mu+\frac{\mu_t}{\sigma_\varepsilon}\right)\frac{\partial\varepsilon}{\partial y}\right]+\frac{\partial}{\partial z}\left[\left(\mu+\frac{\mu_t}{\sigma_\varepsilon}\right)\frac{\partial\varepsilon}{\partial z}\right]+ \tag{13}$$
$$+\rho C_1 S_\varepsilon-\rho C_2\frac{\varepsilon^2}{k+\sqrt{\nu\varepsilon}}+C_{1\varepsilon}\frac{\varepsilon}{k}C_{3\varepsilon}G_b$$

$$\frac{\partial(\rho ku)}{\partial x}+\frac{\partial(\rho kv)}{\partial y}+\frac{\partial(\rho kw)}{\partial z}=\frac{\partial}{\partial x}\left[\left(\mu+\frac{\mu_t}{\sigma_k}\right)\frac{\partial k}{\partial x}\right]+\frac{\partial}{\partial y}\left[\left(\mu+\frac{\mu_t}{\sigma_k}\right)\frac{\partial k}{\partial y}\right]+\frac{\partial}{\partial z}\left[\left(\mu+\frac{\mu_t}{\sigma_k}\right)\frac{\partial k}{\partial z}\right]+ \tag{14}$$
$$+G_k+G_b-\rho\varepsilon-Y_M$$

with μ_t the turbulent viscosity, Pa s; σ_k the turbulent Prandtl number for k; σ_ε the turbulent Prandtl number for ε; G_b the generation of turbulence kinetic energy due to buoyancy, kg m^{-1} s^{-3}; G_k the generation of turbulence kinetic energy due to the mean velocity gradients, kg m^{-1} s^{-3}; Y_M the contribution of the fluctuating dilatation in compressible turbulence to the overall dissipation rate.

The turbulent dynamic viscosity, μ_t, is to be predicted from the knowledge of the turbulent kinetic energy, k, and the turbulent kinetic energy dissipation rate, ε. The transport equations for k and ε are formulated using the realizable k-ε model. They can be derived from Navier-Stokes equations, but the constants in equation (13) are derived using realizable theory, as suggested in [16]. The constants in the model are $C_{1\varepsilon} = 1.44$, $C_2 = 1.9$, $\sigma_k = 1.0$, $\sigma_\varepsilon = 1.2$, $C_{3\varepsilon} = 1$, $C_1 = \max [0.43, \eta/(\eta + 5)]$ with $\eta = S(k/\varepsilon)$, where S is a function of the shear stress tensor [16], for buoyant shear layers for which the main flow direction is aligned with the direction of gravity. For buoyant shear layers that are perpendicular to the gravitational vector, $C_{3\varepsilon} = 0$.

3.1.2. Equations governing the solid domains

A three-dimensional conduction model in the beam and the plasterboard is employed with constant conductivity values. The equation in the steady state regime with constant thermo physical properties is

$$\frac{\partial^2 T_s}{\partial x^2} + \frac{\partial^2 T_s}{\partial y^2} + \frac{\partial^2 T_s}{\partial z^2} = 0 \tag{15}$$

The radiative heat flux leaving a wall is evaluated as the sum of the reflected fraction of the incident heat flux, $\dot{q}_{in}$, and the emitted heat flux

$$\dot{q}_{out} = (1 - \varepsilon_s)\, \dot{q}_{in} + \varepsilon_s\, \sigma\, T_s^4 \tag{16}$$

where

$$\dot{q}_{in} = \int_{s \cdot n > 0} I_{in}\; s \cdot n\; d\Omega \tag{17}$$

with I_{in} the irradiation, W m^{-2}; s the direction of the irradiation; n the normal to the surface; Ω the solid angle, sr.

3.1.3. Boundary conditions

The temperature of the burner is 700 K. The vents are assumed to be black bodies at 300 K, the convective coefficient, h_0, and the temperature, T_0, outside the ceiling are assumed to be 4.0 W K^{-1} m^{-2} and 300 K, respectively. The boundary conditions for the fluid and solid domains are reported in table 3, with reference to figure 3.

3.2. Standalone case

The three-dimensional computational domain is made up by the steel beam and the above part of the plasterboard ceiling. Its section in an *xy* plane is sketched in figure 4.

Gray surfaces and thermo-physical properties of the solids independent of the temperature have been assumed.

Table 3. Boundary conditions for the solid and fluid domains.

Surface	Boundary condition			
	u	*v*	*w*	Temperature
Outside ceiling	0	0	0	$-k_p \frac{\partial T_p}{\partial y} = h_0 \left(T_p - T_0\right)$
Vents	$\frac{\partial u}{\partial x} = 0$	$\frac{\partial v}{\partial x} = 0$	$\frac{\partial w}{\partial x} = 0$	300 K
Vertical walls	0	0	0	300 K
Outside floor	0	0	0	300 K

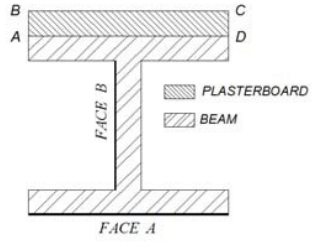

Fig.4 - The computational domain for the standalone case.

Table 4. Boundary conditions for the solid domains.

Surface	Boundary condition
Outside beam surface	$-k_b \frac{\partial T_b}{\partial n} = \varepsilon_b \, \sigma \left(T_b^4 - T_{AST}^4 \right) + h \left(T_b - T_{AST} \right)$
AB and CD plasterboard surfaces	$\mp k_p \frac{\partial T_p}{\partial x} = \varepsilon_p \, \sigma \left(T_p^4 - T_{AST}^4 \right) + h \left(T_p - T_{AST} \right)$
BC plasterboard surface	$-k_p \frac{\partial T_p}{\partial y} = \varepsilon_p \, \sigma \left(T_p^4 - T_0^4 \right) + h \left(T_p - T_0 \right)$

A three-dimensional conduction model in the beam and the plasterboard is employed with constant thermal conductivity values. The equation in the steady state regime with constant thermophysical properties is the above written equation (15).

Boundary conditions for the above mentioned solid domains are reported in table 4, with reference to figure 4.

3.3. Numerical analysis

The commercial Fluent CFD code was employed to solve the governing equations [16]. The SIMPLE scheme was chosen to couple pressure and velocity. The Discrete Transfer Radiation Model (DTRM), that assumes all surfaces to be diffuse, is chosen. The following convergence criteria were assumed: 10^{-3} for the residuals of the velocity components and 10^{-8} for the residuals of the energy. An analysis of sensitivity was conducted in terms of temperature profiles; a 120 ° polar angle and a 48 ° azimuthal angle were chosen for the radiation model as well as a 0.020 m square grid was chosen for the thermo-fluid-dynamic model.

4. Results

In the following the distribution of temperatures, convective coefficients and total heat fluxes released to the beam along significant beam boundaries, predicted for both the conjugate and the standalone cases, are presented.

As to the standalone case, reference was made to three different convective coefficients: the first, h_{conj}, is the local convective coefficient predicted in the conjugate case; the other, h_{25} = 25 W m^{-2} K^{-1} is the average value recommended by the Eurocode [17]; the third, h_{35} = 35 W m^{-2} K^{-1}, is a higher value, accounting for the worst predictable conditions. The emissivities of the beam and plasterboard surfaces are assumed to be 0.80 and 0.40, respectively.

The distribution of the temperature of the fluid, the surface temperature of the beam, the adiabatic surface temperature and the temperature defined in equation (3) as well as the distribution of the convective heat transfer coefficient predicted in this paper for the conjugate case, h_{25} = 25 W m^{-2} K^{-1}, h_{35} = 35 W m^{-2} K^{-1}, both along the bottom horizontal face (A) of the beam, for the conjugate case and for z = 1,240 mm are reported in figures 5 and 6, respectively.

Figure 5 shows that the adiabatic surface temperature assumes values in the $T_{req} \div T_f$ range. We can notice that the surface temperature of the beam is higher than the temperature of the fluid, which, close to the wall, is fairly higher than the temperature of the fluid before the fire ignition. One can, therefore, conclude that in the investigated case the increase in the inner temperature of the beam is due only to the contribution of the radiative heat flux, since convective heat flux from the beam to the fluid balances a fraction of the net radiative heat flux entering the beam.

Figure 6 exhibits a nearly uniform 16 W m^{-2} K^{-1} value of the coefficient of convection along the bottom face of the beam in the conjugate case, lower than the 25 W m^{-2} K^{-1} recommended by the Eurocode and commonly used in the thermo-structural analyses.

The distribution of the total heat fluxes released to the beam predicted in this paper, both for the conjugate case and the standalone cases and for z = 1.24 m, along the bottom horizontal face (A) and the vertical face (B) of the beam is presented in figures 7a and 7b, respectively.

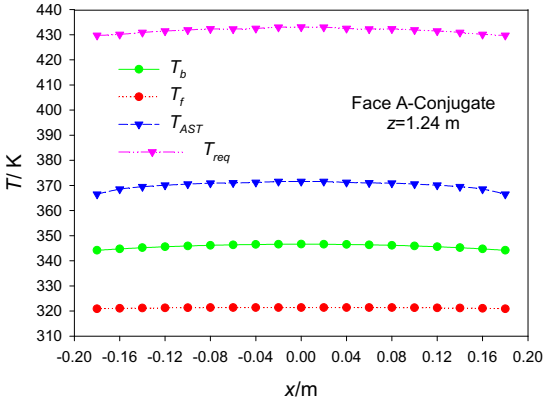

Fig. 5. Temperatures along the face A of the beam.

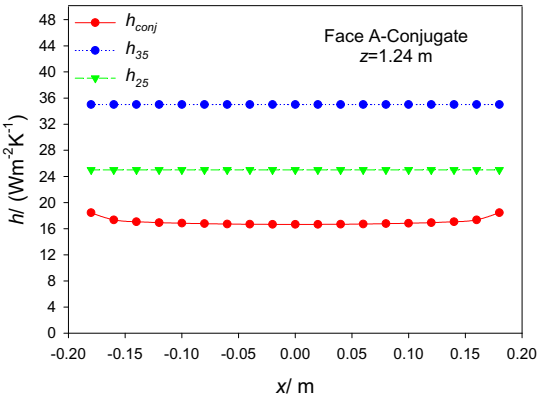

Fig. 6. Convective coefficients along the face A of the beam.

Figure 7 shows that the total heat flux released to the bottom surface of the beam (A), directly facing the burner, is larger than that released to its lateral surface (B), as it was to be expected. Positive values of the total heat flux through the face A denote that the radiative contribution to the heat flux is wherever larger than that of the convective heat flux. On the contrary, negative values of the total heat flux are detected along almost the entire face B of the beam, that is no wonder since the configuration factor between the vertical side of the beam and the burner is null and, therefore, convective heat transfer is mostly involved and the net heat flux exits the beam. The comparison of predictions for the conjugate case with those for the standalone cases exhibits a good agreement only when the h_{conj} coefficient of convection is employed. In the standalone cases the values of the total heat flux predicted using h_{25} and h_{35} are larger than those predicted using h_{conj} because both convection and radiation significantly contribute to heat transfer, with the common external temperature, that is assumed to be the adiabatic surface temperature.

The distribution of the surface temperature of the beam predicted in this paper, both for the conjugate case and the standalone cases and for z = 1.24 m, along the bottom horizontal face (A) and the vertical face (B) of the beam is reported in figures 8a and 8b, respectively. The figure exhibits temperatures of the bottom face of the beam, directly facing the burner, higher than those attained on the lateral face. The comparison between surface temperatures predicted in the conjugate and standalone cases confirms that the agreement is better when in the standalone case h_{conj} is employed. When use is made of h_{25} and h_{35}, the larger the convection coefficient the larger the difference between the predicted values. It is also worth noticing that predictions for the standalone cases overestimate the surface temperatures of face A whereas they underestimate surface temperatures of face B, similarly to what was

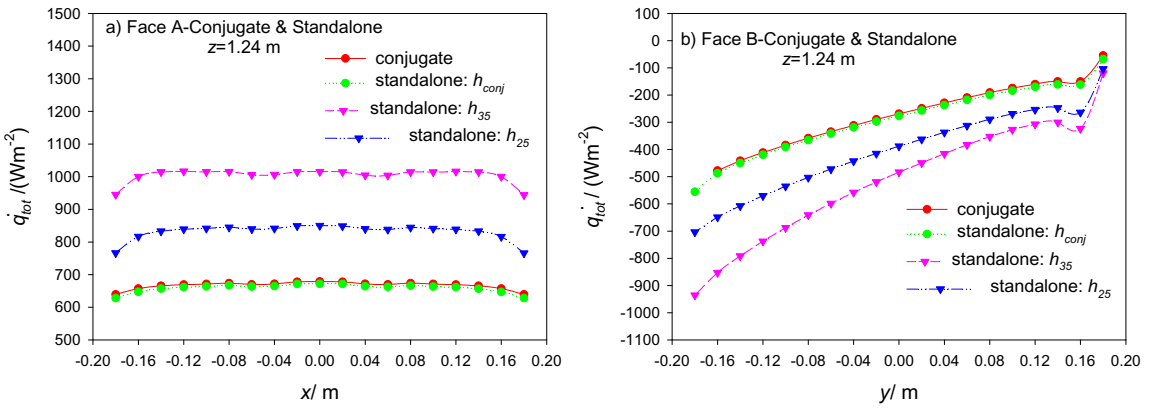

Fig. 7. Total heat flux along two faces of the beam: a) Face A; b) Face B.

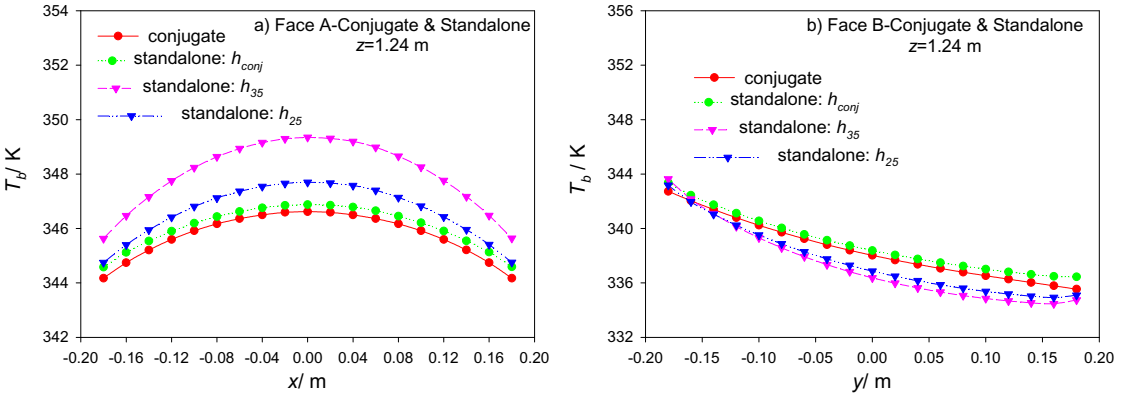

Fig. 8. Temperatures along two faces of the beam: a) Face A; b) Face B.

pointed out for the total heat flux. The percent relative errors in the surface temperature of the beam, e_{T_b}, and in the total heat flux released to the beam, $e_{\dot{q}_{tot}}$, predicted for the standalone cases with respect to their values predicted for the conjugate case, are defined as

$$e_{T_b} = \frac{T_{b,\,stan} - T_{b,\,conj}}{T_{b,\,conj} - T_0} \cdot 100 \qquad e_{\dot{q}_{tot}} = \frac{\dot{q}_{tot,stan} - \dot{q}_{tot,\,conj}}{\dot{q}_{tot,\,conj}} \cdot 100 \tag{18}$$

The distribution of the above errors along the bottom horizontal face (A) and the vertical face (B) of the beam, for z = 1.24 m, is reported in figure 9. The figure allows to compare on a quantitative basis both the total heat flux and surface temperature of the beam predicted in the conjugate case with those predicted in the standalone case.

With reference to the face A, figure 9a points out a minimum relative error in the surface temperature A, equal to nearly 1%, when h_{conj} is employed and a maximum relative error, about 6%, when h_{35} is employed. About 2% and 5% errors in the same temperatures on face B of the beam are exhibited in figure 9b. As far as errors in the total heat flux are concerned, their minimum value on the bottom face A is nearly 2%, with h_{conj}, and the maximum value is about 50% with h_{35}. The correspondent errors on the face B are nearly 7% and 75% (also 125%, somewhere) with h_{conj} and h_{35}, respectively.

5. Conclusions

Adiabatic Surface Temperature (AST) was evaluated in a steel beam located at the ceiling of a room where a fire occurred. A burner was assumed to be located on the room floor in front of the beam. A conjugate and a one way, or "standalone", approach were compared in order to investigate the use of AST as the exchange parameter between thermal fluid-dynamics and structural codes. Relative errors between predictions obtained by means of the conjugate case and the standalone beam case were provided. Results showed that standalone approach well predicts surface temperatures and total heat fluxes, provided the convection coefficients evaluated in the conjugate case were employed. Differences between values predicted with the conjugate case and the standalone case were larger when higher values of the convection coefficient are used. The above differences in the surface temperatures are within 6% whereas those in the total heat flux are up to 75%, with a maximum about 125%.

Acknowledgements

This work was supported by the Ministero della Giustizia with the CUP J63G10000080001 grant.

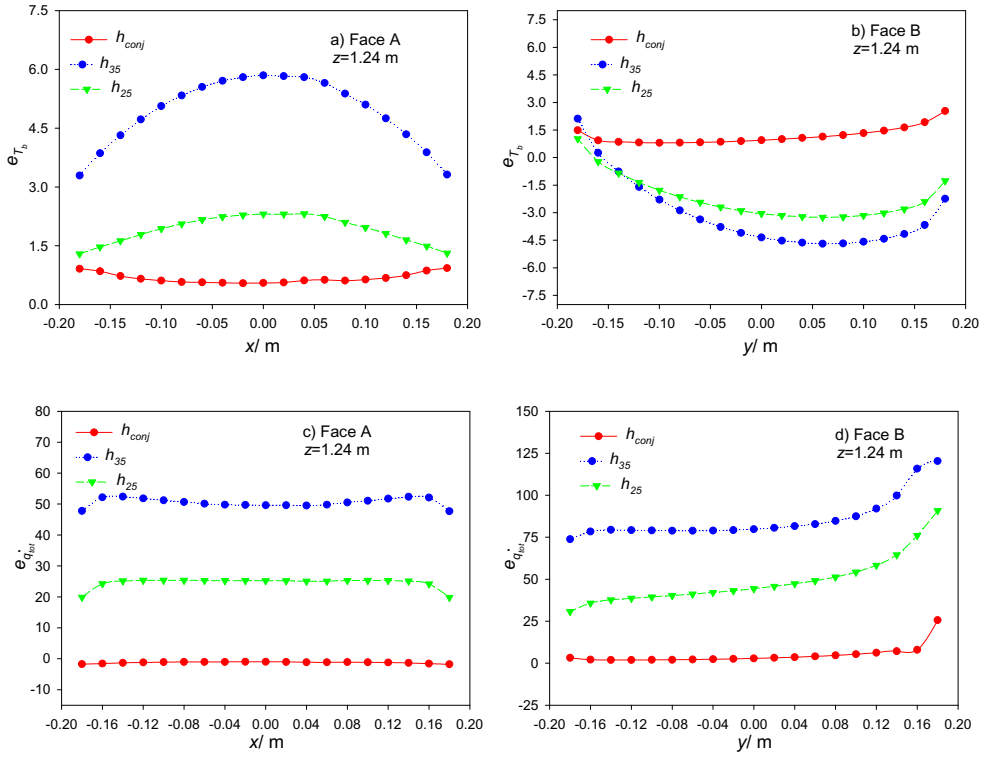

Fig. 9. Relative errors along two faces of the beam: a) surface temperature along Face A;
b) surface temperature along Face B; c) total heat flux along Face A; d) total heat flux along Face B.

References

[1] Federal Emergency Management Autority FEMA. World trade centre building performance study. FEMA. Washington, DC, USA, 2002.
[2] Institution of Structural Engineer ISE, Safety in tall buildings and buildings of large occupancy. Inst. of Structural Engineer, London, 2002.
[3] Prasad K, Baum HR. Coupled fire dynamics and thermal response of complex building structures. *Proc of the Combustion Institute*; 2005;30:255-62.
[4] Usmani AS, Rotter JM, Lamont S, Sanad AM, Gillie M. Fundamental principles of structural behaviour under thermal effect. *Fire Safety J* 2001;36:721–44.
[5] Elghazouli AY, Izzuddin BA. Analytical assessment of the structural performance of composite floors subject to compartment fires. *Fire Safety J* 2001;36:769–94.
[6] Huang Z, Burgess IW, Plank JR. Non-linear structural modelling of a fire test subject to high restraint. *Fire Safety J* 2001;36:795–814.
[7] Noordijk LM, Lemaire AD, Fellinger JHH. (2005a) TNO report "FIRESTRUC WP3 – Data exchange and communication between VESTA and DIANA for two-way coupled thermal analysis", August 2005.
[8] FIRESTRUC – Integrating advanced three-dimensional modelling methodologies for predicting thermo-mechanical behaviour of steel and composite structures subjected to natural fires, RFCS project RFS-PR-02110, European Commission report, 2008.
[9] Franssen JM. A thermal/structural program modelling structures under fire. *Eng. J* 2005;42 3:143-58.
[10] Watson D., Philip G. A refinement of inverse distance weighted interpolation. *Geo-Processing* 1985;2: 315-27.
[11] Ren A, Shi J, Shi W. Integration of fire simulation and structural analysis for safety evaluation of gymnasiums — with a case study of gymnasium for Olympic Games in 2008. *Automation in Construction J*, 2007;16: 277–89.
[12] Wickström U, Duthinh D, McGrattan K. Adiabatic surface temperature for calculating heat transfer to fires exposed structures. Proc. 11th Int. Interflam Conf.Sept. 3-5, 2007; London, England, 943-53.
[13] Wickström U, Robbin A, Baker G. The use of Adiabatic Surface Temperature to design structures for fire exposure. *J Structural Fire Eng* 2011; 2:21-8.
[14] Bystrom A, Cheng X, Wickström U, Veljkovic M. Measurement and calculation of Adiabatic Surface Temperature in a full-scale compartment fire experiment. *J Fire Sciences* 2013;31:35-50.
[15] Andreozzi A, Bianco N, Musto M, Rotondo G. Influence of wall emissivity and convective heat transfer coefficient on the adiabatic surface temperature as thermal/structural parameter in fire modeling. *Applied Thermal Engineering* 2013; 51:573-85.
[16] Fluent user's guide, Fluent Inc., 2005.
[17] EN 1993-1-2. Eurocode 3: design of steel structures — part 1–2: general rules — structural fire design. London: British Standard Inst. 2005.